Advances in Science and Technology Research Journal

*Advances in Science and Technology Research Journal*, 2025, 19(6), 94–107
https://doi.org/10.12913/22998624/202851
ISSN 2299-8624, License CC-BY 4.0

Received: 2025.03.02
Accepted: 2025.04.15
Published: 2025.05.01

# Effect of additional Titanium diboride on characteristic of Ti-24Nb-4Zr-8Sn alloy

Hussein Khalil Burhan[1*], Jassim Mohammed Salman[1], Nawal Mohammed Dawood[1]

[1] College of Materials Engineering, University of Babylon, Iraq
* Corresponding author's e-mail: mat576.hussien.kaleel@student.uobabylon.edu.iq

## ABSTRACT

Titanium and its alloys have low density, superior resistance of corrosion and high specific strength, also found extensive use in the aerospace, petrochemical, biomedical, and many other industries. Because metastable β-titanium alloys with b stabilizing elements like Nb and Zr provide a great mix of low modulus and high strength, they are particularly desirable as implant materials. Titanium diboride $TiB_2$, is a very hard ceramic with superior wear resistance, oxidation stability, and heat conductivity. The purpose of this research is to estimate the influence of $TiB_2$ at several percentages (0.1, 0.2, 0.3, and 0.4 wt.%) on the Ti2448 alloy fabricated by powder metallurgy, macrostructures, and mechanical characteristics of powder-metallurgically produced Ti-24Nb-4Zr-8Sn-$TiB_2$ composites. According to the experimental findings, the hardness rises as the percentage of $TiB_2$ grows, reaching 166 HB at 0.4 wt.% addition, while the wet wear rate falls as the $TiB_2$ content increases, reaching $7.09\times10^{-5}$g/cm.

**Keywords:** wear rate, biomedical material, Ti-24Nb-4Zr-8Sn alloy, and powder metallurgy.

## INTRODUCTION

Titanium alloys are now usually used in applications of biomedical because of its excellent corrosion resistance, exceptional biocompatibility, low elastic modulus, and high specific strength. As implant materials, they are frequently utilized. Nevertheless, there are issues with the use of traditional titanium alloys as well. These include commercial pure titanium CP-Ti, Ti-6Al-4V and Ti-Ni alloy [1, 2]. The alloying elements Ni, Al, and V are poisonous and allergic on the one hand. These metals can cause allergic reactions, a range of illnesses, including problems with the nervous system and Alzheimer's disease, when corrosion causes them to be released into the human body [3]. Their CP-Ti elastic moduli of 105~110 GPa and Ti-6Al-4V elastic moduli of ~110 GPa remain abnormally large. nevertheless, in contrast to human bones(12~30 GPa) [4]. In human bodies, stress shielding caused by orthopedic implants with the mismatched of elastic moduli can result in implant loosening or bone fractures after implantation. In an attempt to solve the aforementioned problems, Recently, a new generation of medical titanium alloys has been produced that are non-toxic, have a lower modulus, and are better biocompatible [4, 5].

Due to its comparatively high values of a well-known ceramic material with comparatively high durability and strength is titanium diboride ($TiB_2$); its properties include hardness, strength to density ratio, wear resistance, and melting point [6]. $TiB_2$ single crystal displays a hexagonal symmetry, as illustrated in Figure1.

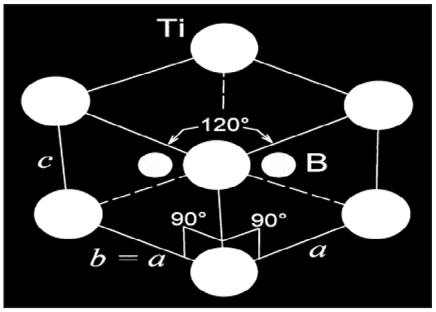


**Figure 1.** The unit cell of single crystal $TiB_2$ in a hexagonal form [7]

$TiB_2$ is significantly stronger in compression than it is under flexure or tension, similar to most of structural ceramics. There is really little data available [7, 8].

High hardness (25 GPa), excellent electrical conductivity (22 × 106 Ω $cm^{-1}$), low density (4.5 g/$cm^3$), good thermal conduction (96 W/(m·K)), and high melting point (3225 °C) are all characteristics of titanium diboride. One of the advantages of materials for wear applications and high-temperature structural applications is chemical stability [9]. When combined with the above high temperature characteristics, boron's neutron absorption property makes $TiB_2$ the perfect option for controller rod material in nuclear reactors operating at high temperatures. For the production of $TiB_2$, titanium oxide and boron mixed oxides can be carbothermically reduced, titanium oxide can be reduced by carbon and boron carbide, and the mixed oxides can be reduced by metals like silicon, magnesium, aluminum, etc. or by mechanical alloying, heating, or self-propagating high temperature synthesis (SHS). from the constituent elements [10–15]. When boron carbide reduces titanium oxide, the reaction that results is as follows:

$$2TiO_2 + B_4C + 3C \rightarrow 2TiB_2 + 4CO \quad (1)$$

Niinomi et al. [16] studied the when (0.1 and 0.2) mass percent B and (0.2 and 0.5) mass percent Y were added, TNTZ demonstrated a good compromise between ductility (elongation) and strength (tensile strength). when different quantities of additional $TiB_2$ and $Y_2O_3$ were cold-rolled after solution treatment to assess their mechanical characteristics, including fatigue strength, Young's modulus, and tensile properties. When the Young's modulus is low, a tiny amount of $TiB_2$ and Y203 can be added to TNTZ to increase its fatigue strength.

Zhang et al. [17] An acetabular cup sample and other biomedical β alloy Ti–24Nb–4Zr–8Sn components were made using selective laser melting (SLM). Furthermore, the mechanical properties of the raw material were compared with those of conventionally processed materials.

Using MIM, Fırat et al. [18] satisfactorily evaluated samples of Ti–24Nb–4Zr–8Sn alloys with varied plastic elongation ranging from 2% to 9% depending on sintering circumstances and an ultimate tensile strength around 655 and 720 MPa. At 54 GPa, The lowest Young's modulus is over 50% fewer than that of Ti–6Al–4V and (CP Ti).

The objective of this work is to create the Ti2448 alloy using a powder metallurgy process and determine the impact of adding $TiB_2$ in varying ratios on the mechanical properties and microstructural evaluation of the sintered specimens.

## EXPERIMENTAL

### Raw materials

Table 1 describes the average particle size and the purity of the materials powders used in preparation, along with their test results, and Figure 2 to 6 show particle size analyses for Ti, Nb, Zr, Sn and $TiB_2$ Powders.

Ti-24Nb-4Zr-8Sn, often referred to as Ti2448, titanium diboride was used as a raw material to make biomedical composites in varying percentages (0.1, 0.2, 0.3, and 0.4 wt.%). The composition and code of the alloys employed in this study are described in detail in Table 2.

For best results, metallic powders requirement be thoroughly homogenized before compaction and sintering. The process of blending includes mixing powders with the same composition but perhaps different particle sizes using the following device.

To reduce porosity, different particle sizes are frequently mixed at MTI corporation's top planetary automatic ball mill. On the other hand, mixing is defined as the act of blending powders of more than one material [19]. A planetary automated

**Table 1.** The typical powder particle size and purity

| Material (powder) | Purity % | Average particle size (μm) | Source |
|---|---|---|---|
| Ti | 99.5 | 47 | Qingdao Hesiway Industrial Co., Ltd. China |
| Nb | 99.9 | 19 | Sichuan Porous Metal Technology CO., LTD. China |
| Zr | 99 | 24 | Xian Function Material Group CO., LTD. P.R.China |
| Sn | 99.9 | 11 | Alpha Chemika Inc., India |
| $TiB_2$ | 98.5 | 6 | Nanografi Nano Technology, Ankara, Türkiye |

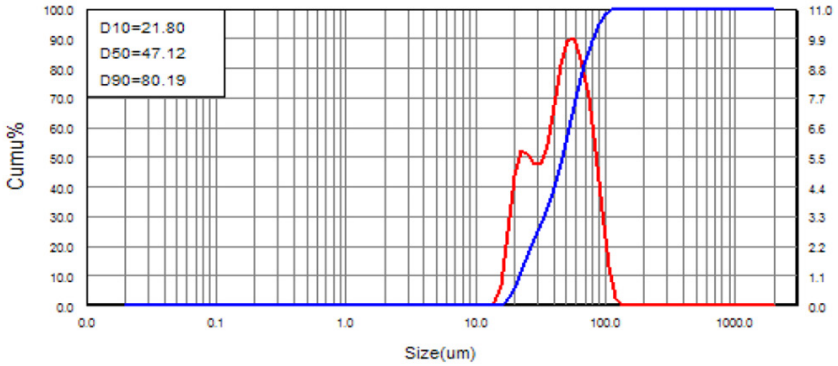


**Figure 2.** Particle size analyses for Ti powder

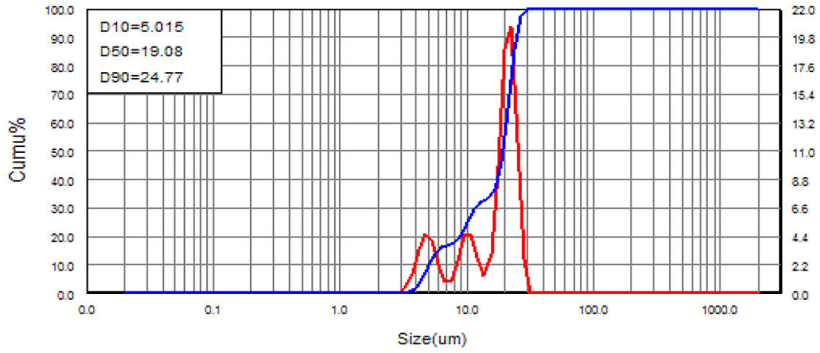


**Figure 3.** Particle size analyses for Nb powder

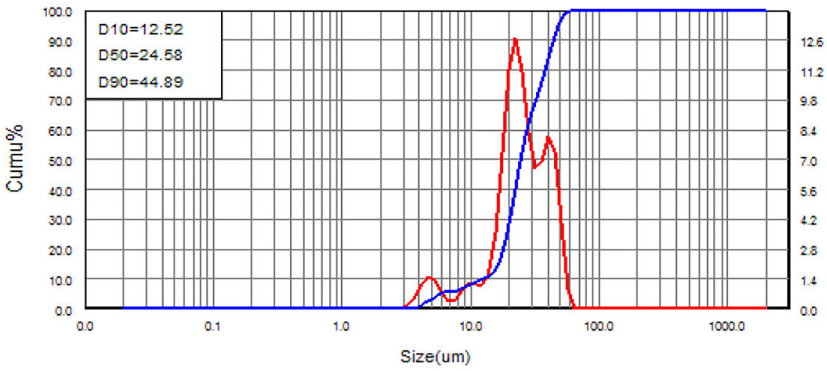


**Figure 4.** Particle size analyses for Zr powder

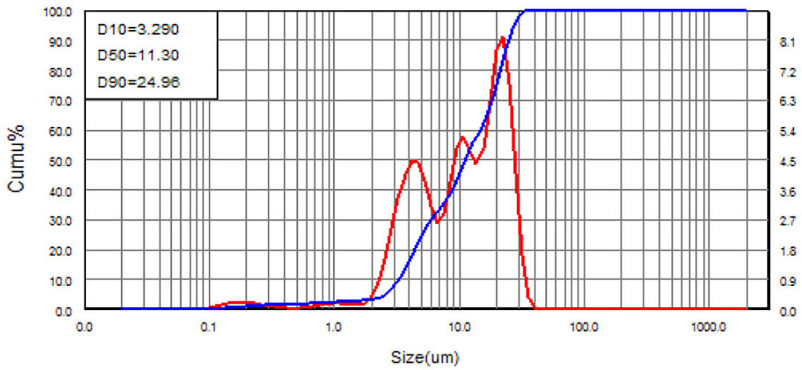


**Figure 5.** Particle size analyses for Sn powder

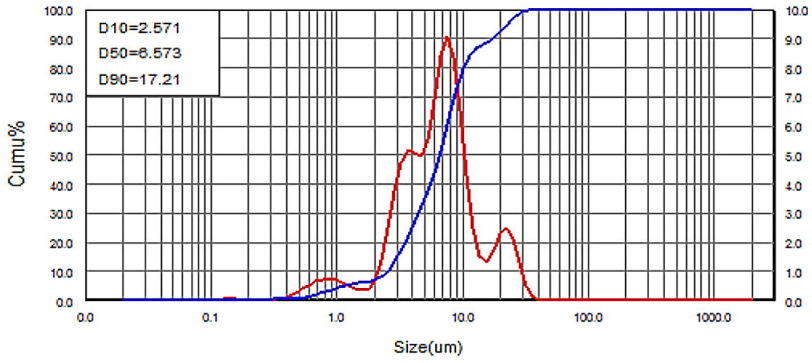


**Figure 6.** Particle size analyses for $TiB_2$ powder

**Table 2.** Alloys' codes and compositions

| Code | Chemical composition (wt.%) |
|---|---|
| M | Ti-24Nb-4Zr-8Sn |
| $A_1$ | Ti-24Nb-4Zr-8Sn+0.1 $TiB_2$ |
| $A_2$ | Ti-24Nb-4Zr-8Sn+0.2 $TiB_2$ |
| $A_3$ | Ti-24Nb-4Zr-8Sn+0.3 $TiB_2$ |
| $A_4$ | Ti-24Nb-4Zr-8Sn+0.4 $TiB_2$ |

ball mill was employed for the wet mixing of powders, utilizing balls made with stainless steel of various sizes for 5 hours to achieve uniform dispersion of the powder particles. The added of acetone was to moisten the mixing medium.

To carry out the compacting process, The mold used was 12.5 mm in diameter and made of stainless steel. Four grams of mixture were compressed under pressure using an electric-hydraulic press that used a single channel device (American, CT340_CT440, type – 800 MPa). A disk spaceman measuring 12.5 mm in diameter and 4.5 mm in thickness was constructed in 4 minutes. To reduce friction, paraffin is lubricated throughout the pressing process.

In order to avoid the specimen from oxidizing, the sintering procedure was conducted The material had to be heated from 25 °C to 1250 °C at a rate of 5 °C each minute in a tube furnace and leaving it in an argon environment for seven hours. After that, gradually cool to room temperature in the furnace while maintaining argon conditions.

With grit sizes of 120, 220, 320, 400, 600, 800, 1000, 2000, and 3000 μm, silicon carbide (SiC) emery sheets were used, the sample's surface was grinding to create substrates. After that, distilled water was used to clean the substrate. The substrates were then polished to a mirror-like smooth finish using a 1.5 μm diamond paste and a grinding and polishing equipment. In accordance with ASTM [20], 92 milliliters of distilled water, 6 milliliters of $HNO_3$, and 2 milliliters of HF were used for the room temperature etching. To be ready for microstructure analysis using the etching process. For three to five seconds the usable samples were immersed in the etching solution. After that, distilled water was used to wash and dry them.

## Phase identification

In the present study, the powder (Ti, Nb, Zr, Sn, and $TiB_2$) was described using the X-ray diffraction analysis test (XRD 6000, Shimadzo, Japan) as well as substrate alloy and reinforced samples. The XRD was performed at a power of Kv/30 mA using Cu Kα radiation (λ = 1.5405 ″). With a scanning rate of 6 degrees per minute and step 0.02 degrees.

## Microstructure test

After the grains were grinding, polished, and etched in a solution, the microscopic structure was analyzed using optical microscopy of the BEL PHOTONICS type to determine the phases that developed and to assess the size and shape of the grains. Scanning electron microscopy (SEM) has been one of the most widely used techniques for surface research since its inception because it makes a large range of sizes and characteristics visible. The microstructure of the reinforcement and matrix was revealed in the current experiment using a SEM type VEGA 3 SBU. It served to clarify the microstructure and morphology of the sintered samples. Energy-dispersive spectroscopy was the

analytical method utilized for elemental and chemical investigation of the implant's surface following sintering.

### Mechanical test

The samples' hardness was measured using a Brinell tester, which was made in Germany. A ball with a diameter of 2.5 mm, an applied force of measurement was performed using 31.25 kg/mm$^2$ and a 10-second implantation time under applied weight circumstances. Three measurements were made for each sample, and the average behavior of the alloys was then analyzed.

Tribology is the technology and science of two surfaces interacting when subjects and activities change. Wear is one of the primary reasons for material waste or a decline in mechanical performance, therefore lowering it could ultimately save a significant amount of money. Friction is the primary cause of wear and dissipated energy [21]. A particular wet wear rate was established with the Pin-on-Disk tribometer model MT/60/H, a sort of pin-on-disc device. Table 3 provides an example of how SBF solution performs the test.

The initial weight was determined by measuring the weight of the substrate. Making sure the specimen's end surface was parallel to the disc surface, it was placed within the holder. The desired wear track radius of 6 mm was achieved by adjusting the holder. 10 N, 15 N, and 20 N loads were used. Prior to the test, the specimen is weighed using a delicate balance. At 350 rpm of spin, after the specified duration of 5, 10, 15, 20, 25, 30, 35, and 40 minutes. The procedure is repeated until forty minutes have passed. The wear rate was calculated as follows [23]:

$$\textit{Specific wear rate} = \Delta W/S \text{ (g/cm)} \qquad (2)$$

**Table 3.** The SBF solutions' chemical composition [22]

| Chemical formula | Quantity |
|---|---|
| NaCl | 6.547 |
| Na $HCO_3$ | 2.268 |
| KCl | 0.373 |
| $MgCl_2 \cdot 6H_2O$- | 0.305 |
| $CaCl_2 \cdot 2H_2O$ | 0.368 |
| $Na_2HPO_4 \cdot 2H_2O$ | 0.178 |
| $Na_2SO_4$ | 0.071 |
| $(CH_2OH)_3CNH_2$ | 6.057 |

where: $\Delta W$ – weight lost (g), $S$ – sliding distance (260 m).

$$S = \textit{Sliding velocity} \text{ (m/s)} \times \textit{time} \text{ (s)} \qquad (3)$$

$$\textit{Sliding velocity} = \pi DN/(30\times1000) \text{ (mm/min)} \qquad (4)$$

where: $D$ – wear track diameter of 10 mm was used, $N$ – speed of rotation disk (350 rpm).

## THE RESULTS AND DISCUSSION

### X-ray diffraction (XRD) analysis of the samples and powders

In order to verify the type of powder as indicated in Figure 7, of the pure powders XRD for Ti, Nb, Zr, Sn, and MWCNT was performed. By comparing the JCPDS card numbers with conventional reference patterns, the phases were identified. The phase identification of the Ti-24Nb-4Zr-8Sn alloy substrate before $TiB_2$ reinforcement is shown in Figure 8a, where beta (β) is the only discernible primary phase. The crystalline planes indicated on JCPDS card No. 44-1288 match the β diffraction pattern, confirming the existence of the β phase can be seen in Figures 8b through e). The XRD patterns also verify that the $TiB_2$/Ti composites made using the powder metallurgy technique were free of extra contaminants.

### Light optical microscope (LOM)

Because a material's behavior is greatly influenced by the size, shape, and distribution of its particles, metallography provides insight into the microstructure of the material and how it relates to its properties [24]. The compressed samples were grind, polished, and etched after being sintered for seven hours at a temperature of 1250 °C. The samples are then subjected to optical microstructure images of the (Ti-24Nb-4Zr-8Sn) alloy with and without addition, The microstructure of etched alloys following an 80x sintering operation is depicted in Figure 9. Grain boundaries, various sized holes, and the current phases were visible in the alloys' microstructure. As seen in Figures 9, the microstructure shows that the β phase forms the majority of the alloys in the material. The dark area results from the existence of the Nb element. (also known as the β-phase) to appear because Nb acts as a stabilizer of beta elements.as depicted in figures:

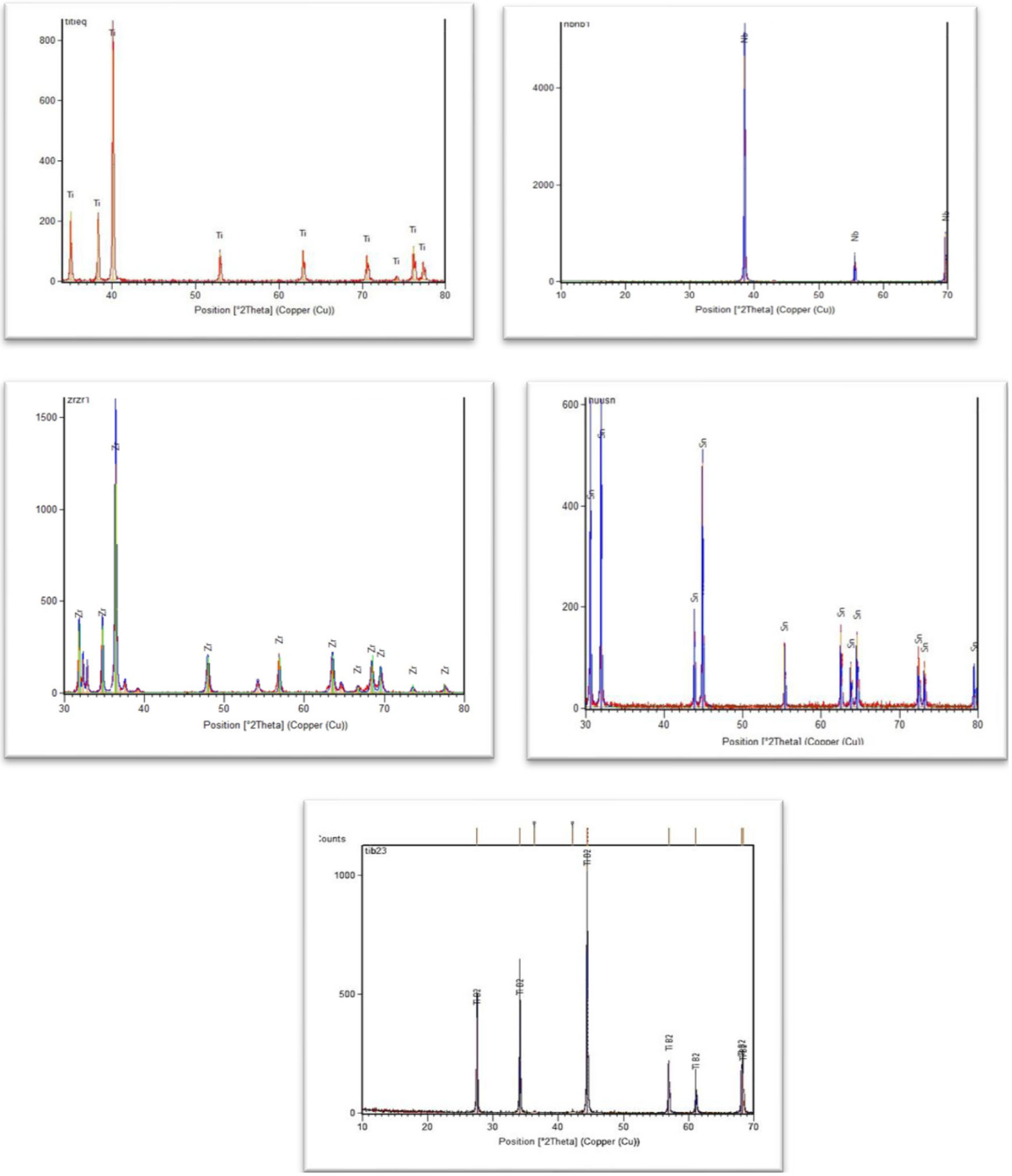


**Figure 7.** XRD pattern of pure material a) Ti, b)Nb, c) Zr, d) Sn, e)$TiB_2$ powder

## Scanning electron microscopy of the samples

In a SEM, incoming electrons impart enough energy to cause secondary electrons to be released from the material. The surface's topography largely determines the secondary electrons' intensity. by measuring the current produced by secondary electrons while the electron beam is moving across the samples. The findings of the SEM microstructure specimen in Figure 10 demonstrate the surface shape of the Ti-24Nb-4Zr-8Sn alloy strengthened by varying titanium diboride percentages. The SEM of the Ti-24Nb-4Zr-8Sn alloy (M) basic alloy without addition is displayed in Figure 10a, whereas Figures 10b to 10e display the alloy reinforced with TiB2. The XRD results were confirmed by The microstructure of sintered samples showed two phases, mainly β and secondary α, forming a multiphase structure [25].

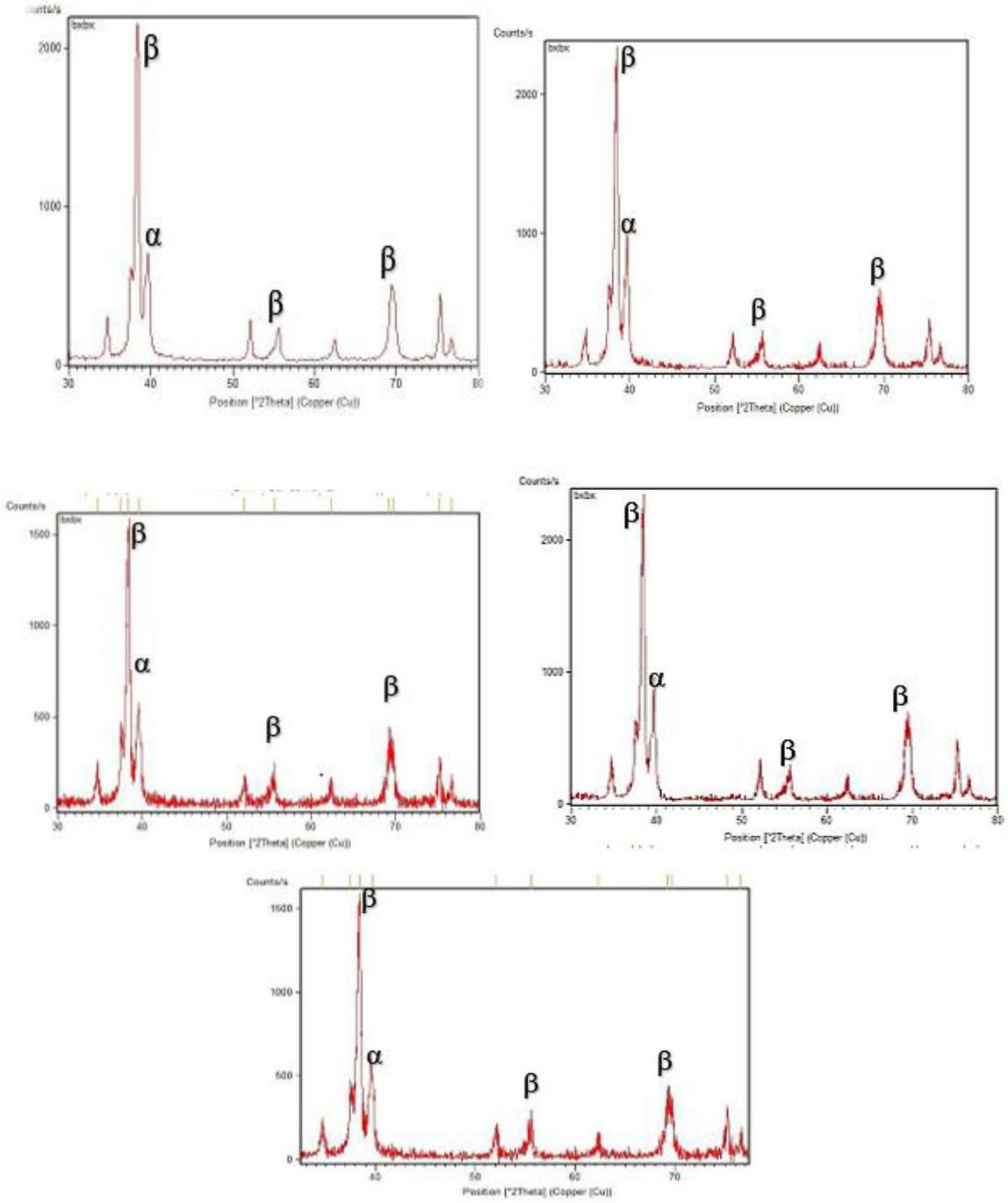


**Figure 8.** XRD for alloy a) M. b)A1, c)A2, d)A3 and e)A4

## Energy dispersive X-ray (EDX) spectroscopy

With EDS, it is possible to identify the chemical composition which results from changes in difference topography on a SEM image. The precision that can be measured from samples is limited by statistical error. EDS was scanned on a range of polished specimens. Given that the EDS study's values only encompass the region where electron touched the surface, as seen in Figures 11–15, The different between the percentage that addition and the analyzing was because of the single point may result in a region that is richer or poorer in a specific element compared to the overall composition, while the presence of Cl in Figure 15 due to used EDX instead of WDX which led to peak overlaps. Boron very close to Lα of chlorine.

## Brinell hardness test

The top, middle, and bottom sections of each sample were tested for hardness, and the

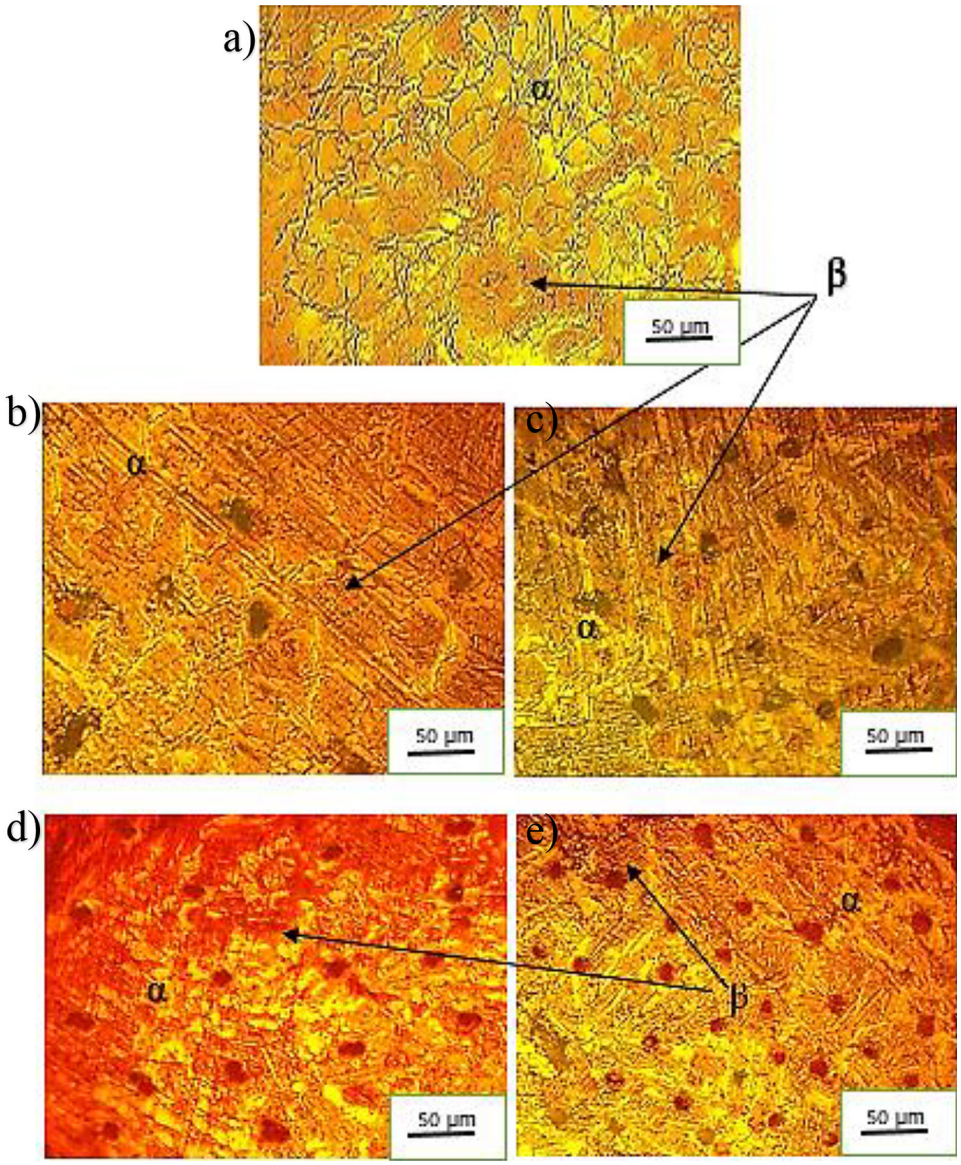


**Figure 9.** Magnified optical micrographs of alloys a) M, b) A1, c) A2, d) A3, and e) A4 (80X)

average of the three measurements was then recorded for each specimen. Hardness increment for specimens as the proportion of $TiB_2$ rises. Figure 16 displays the values of hardness in proportion to the quantity of $TiB_2$ reinforcing. In reality, during plastic deformation suitable for increasing hardness, reinforcements stop dislocation motion [26].

## Wear test

An implant's resistance to wear is one of its essential mechanical characteristics since Wear failure is a major contributor to implant failure. The wear mass loss of test samples was measured under (10, 15, and 20 N) loads over several durations (5, 10, 15, 20, 25, 30, 35, and 40 min), and the wear rates were calculated using the pin-on-disc sliding wear test. The results showed that as loading time increments, In general, the wear rate dropped. The production of stable oxides ($ZrO_2$ and $Nb_2O_5$) on the Ti2448 alloy as a result of dissolution in the SBF solution environment is the reason for this behavior, providing enhanced wear resistance [27–28].

Though the addition of the reinforcing particles to alloy, the wear rate is reducing because of it prevents the material from plastic deformation. This can be caused by the fact that the movement of the matrix and grain boundaries were restricted when $TiB_2$ particles were added to the base alloy. resulting in increased wear resistance, hardness, and decreased volume loss. The inclusion of hard ceramic fibers or particles significantly increases

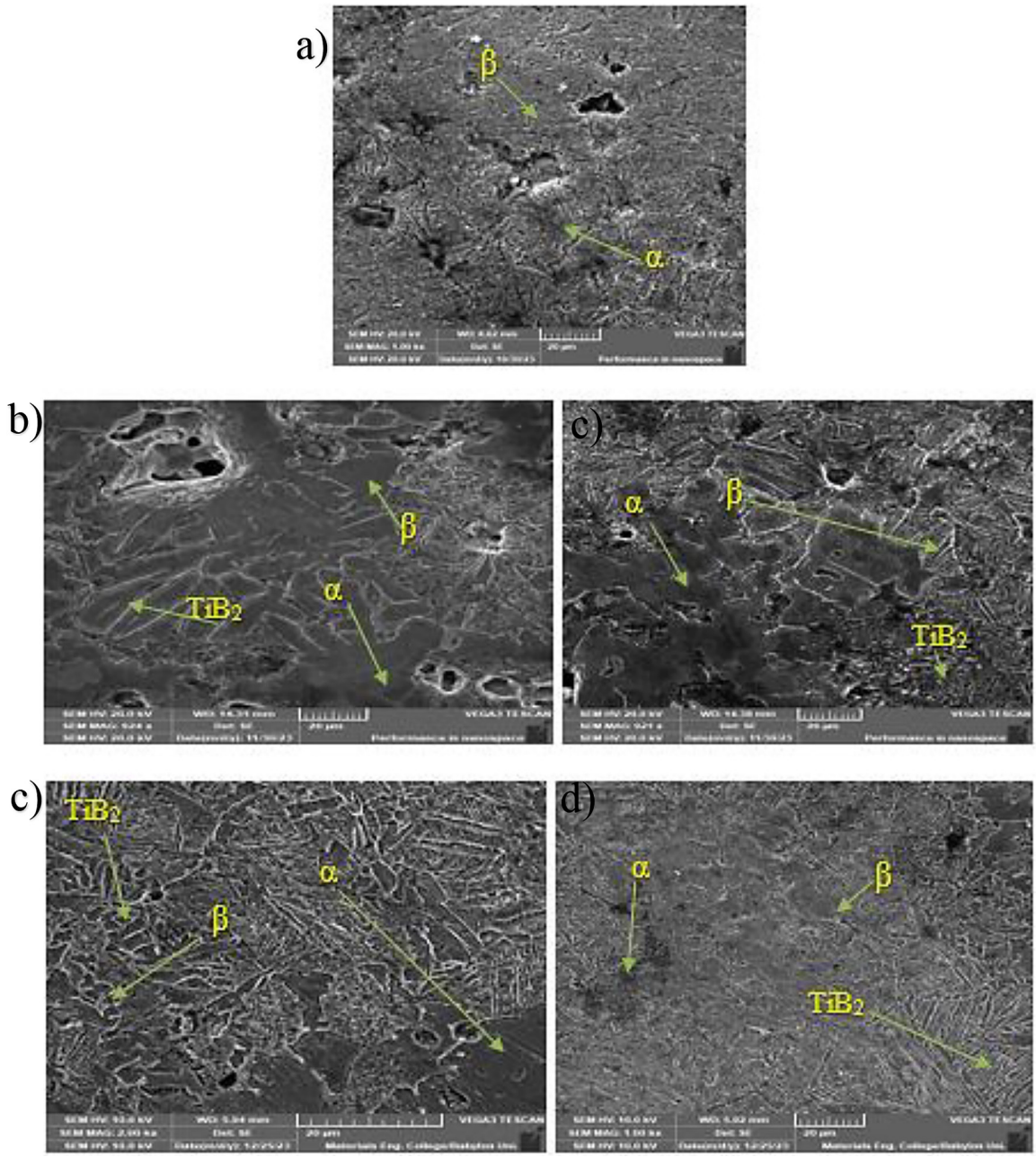


**Figure 10.** Samples a) M, b) A1, c) A2, d) A3, and e) A4 as seen in SEM micrographs

the hardness of the ductile titanium matrix, and this effect is directly correlated with the volume percentage of ceramic reinforcement [29] as seen in Figures (17–19).

## CONCLUSIONS

The titanium alloy used in this study, which has the composition Ti-24Nb-4Zr-8Sn(wt.%), was created via powder metallurgy with element powders and heated to 1250 °C for seven hours. The powder are mixtures with different percentage of titanium diboride (0.1, 0.2, 0.3 and 0.4%) as a reinforce particle, the microstructural and mechanical properties of the samples are studied. The result of Optical, XRD and SEM appear small amount of alpha and mainly beta phase due to the effect of Nb as the stabilizer of beta phase. The results of the hardness and wet wear of alloy showed that the addition of $TiB_2$ enhanced by addition a small quantity and increased by increasing the addition percentage due to distributed of $TiB_2$ particle along the grain boundaries of the matrix led to prevent dislocation motion. Based on the conclusions drawn,

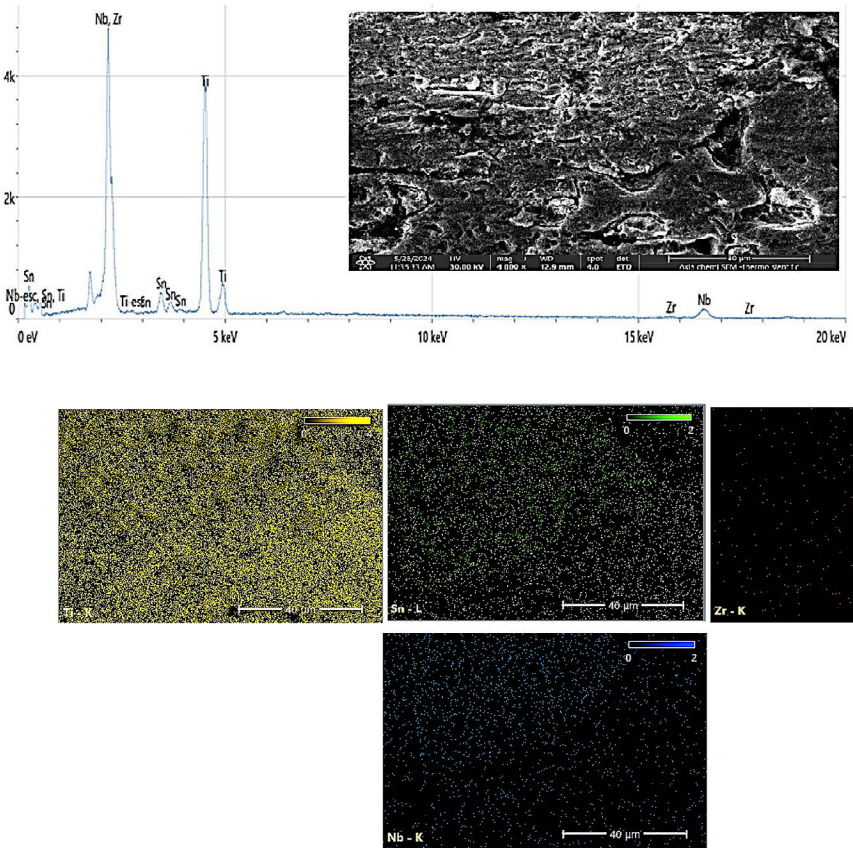


| Element | Weight % |
|---|---|
| Ti | 49.9 |
| Zr | 2.0 |
| Nb | 38.6 |
| Sn | 9.5 |

**Figure 11.** EDS for M alloy

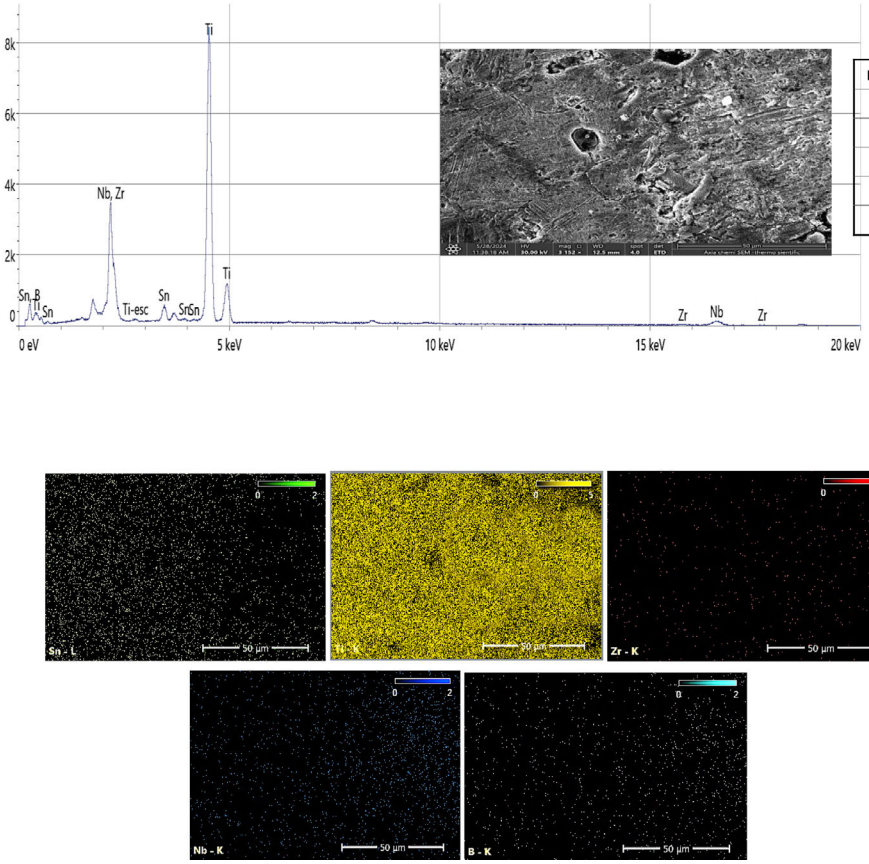


| Element | Weight % |
|---|---|
| B | 17.0 |
| Ti | 52.3 |
| Zr | 1.8 |
| Nb | 21.8 |
| Sn | 7.1 |

**Figure 12.** EDS for A1 alloy

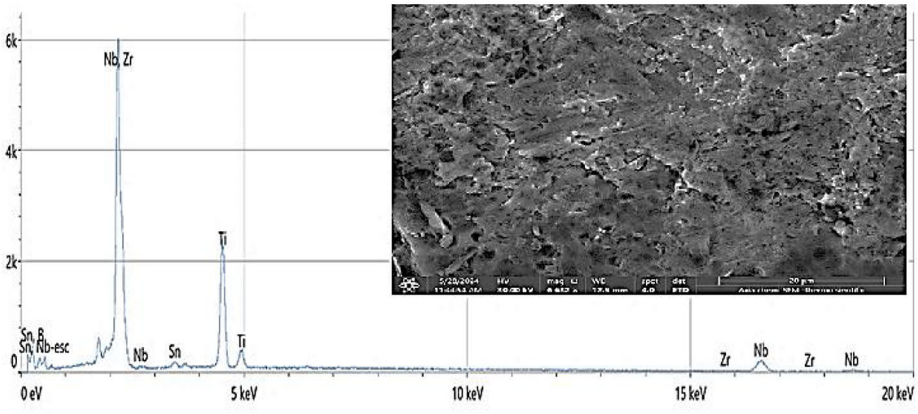


| Element | Weight % |
|---|---|
| B | 16.8 |
| Ti | 36.1 |
| Zr | 6.2 |
| Nb | 36.7 |
| Sn | 4.2 |

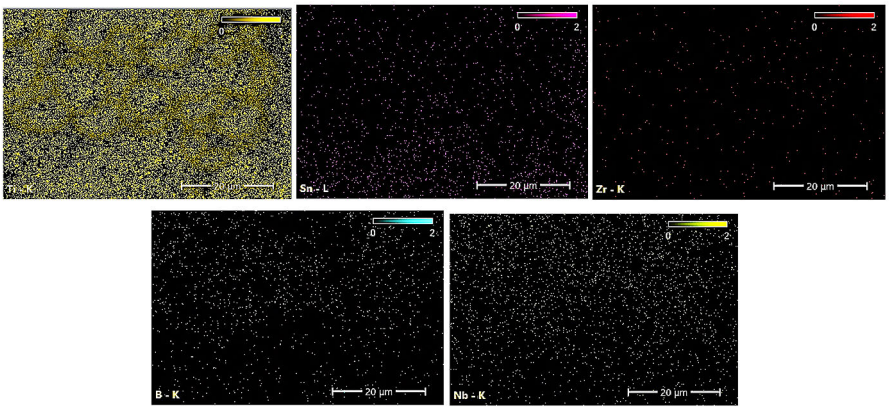


**Figure 13.** EDS for A2 alloy

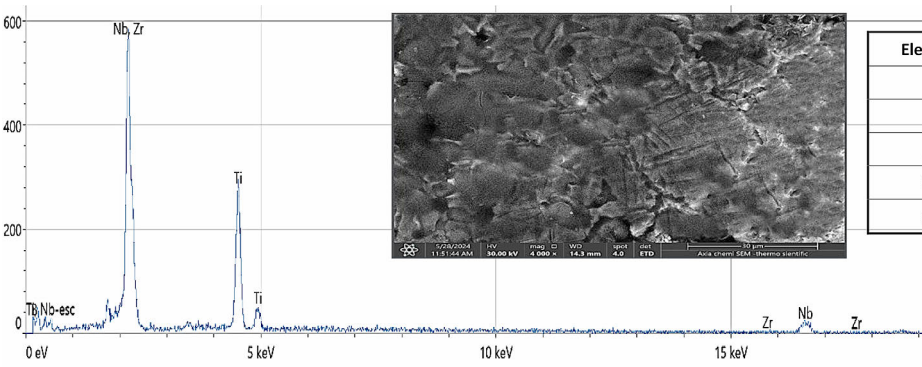


| Element | Weight % |
|---|---|
| B | 3.6 |
| Ti | 37.9 |
| Zr | 1.3 |
| Nb | 53.2 |
| Sn | 4.0 |

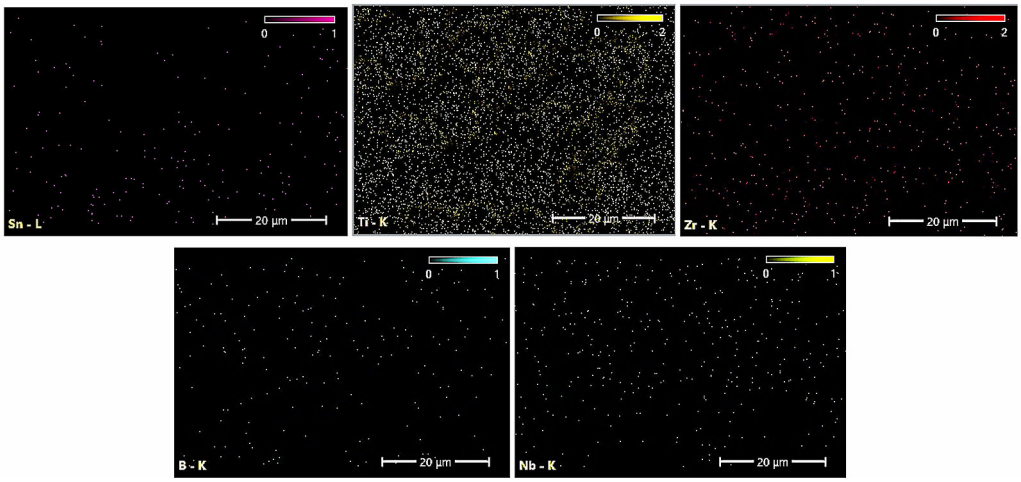


**Figure 14.** EDS for A3 alloy

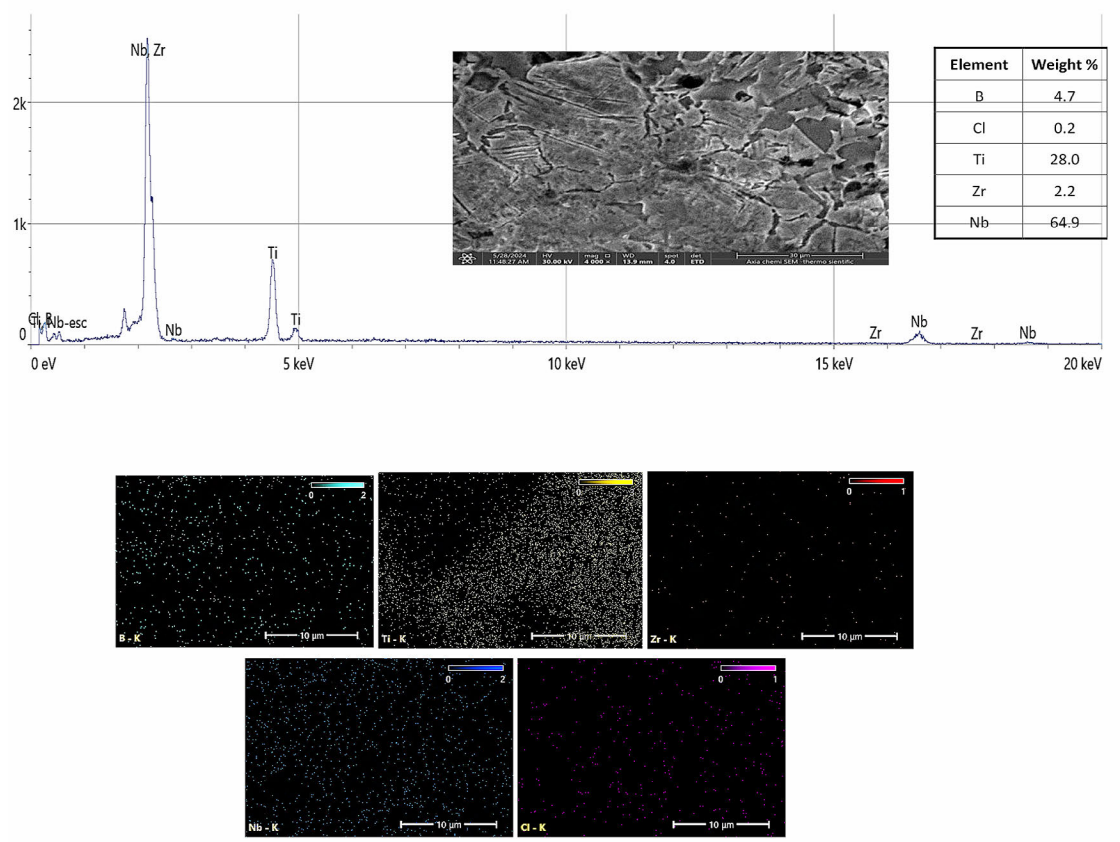


**Figure 15.** EDS for A4 alloy

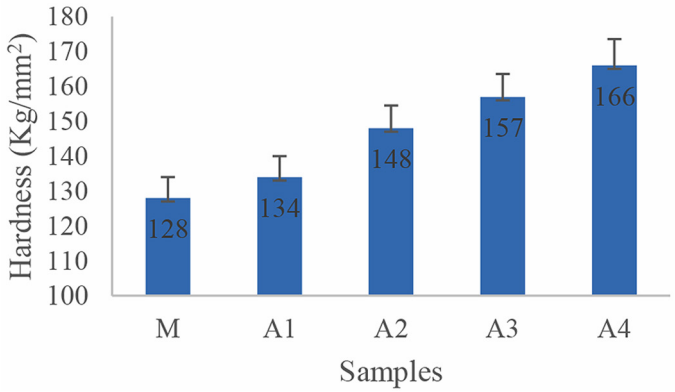


**Figure 16.** Effect of $TiB_2$ contented on hardness for Ti-24Nb-4Zr-8Sn alloy

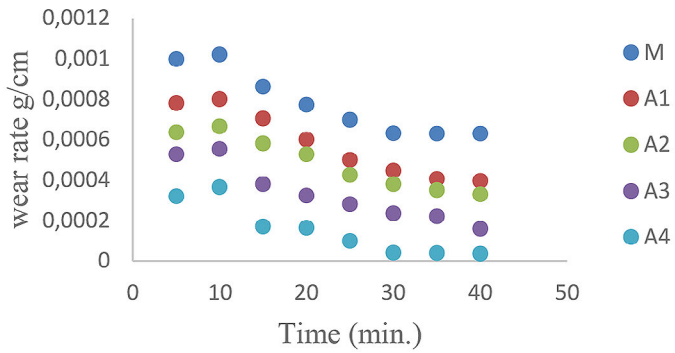


**Figure 17.** Association between wear rate and test time for Ti2448 alloy reinforced by different percentage of $TiB_2$ under 10N Load

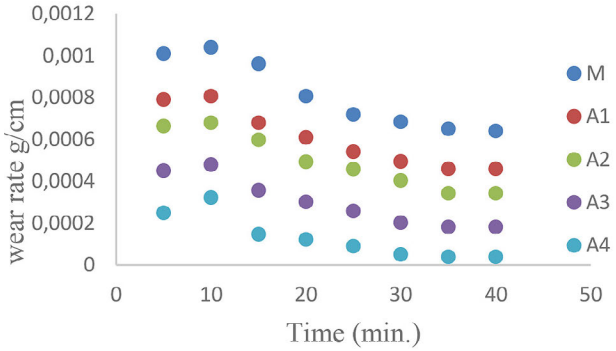


**Figure 18.** Association between wear rate and test time for Ti2448 alloy reinforced by different percentage of $TiB_2$ under 15N Load

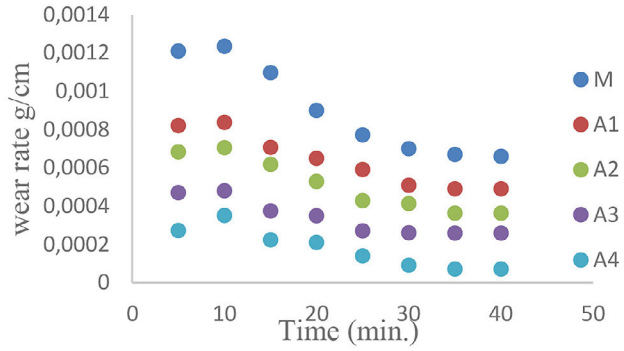


**Figure 19.** Association between wear rate and test time for Ti2448 alloy reinforced by different percentage of $TiB_2$ under 20N Load

the study comes out with the following suggestion for future research investigating the influence addition of $TiO_2$ and ZnO and Investigate how cold work, or rolling, affects the mechanical characteristics of Ti2448 alloy.

## REFERENCES

1. Li H. F., Qiu K. J., Zhou F. Y., Li L., Zheng Y. F. Design and development of novel antibacterial Ti-Ni-Cu shape memory alloys for biomedical application, Scientific Reports 2016; 6: 37475.
2. Bolzoni L., Ruiznavas E.M., Gordo E. Feasibility study of the production of biomedical Ti-6Al-4V alloy by powder metallurgy, Materials Science & Engineering C Materials for Biological Applications 2015; 49(3): 400–407.
3. Genchi G. et al. Nickel: Human health and environmental toxicology. International journal of environmental research and public health 2020; 17(3): 679.
4. Hamidi M. F. F. A., Harun W. S. W., Samykano M., Ghani S. A. C., Ghazalli Z., Ahmad F., Sulong A. B. A review of biocompatible metal injection moulding process parameters for biomedical applications, Materials Science & Engineering C 2017; 78: 1263–1276.
5. Yilmazer H., Niinomi M., Nakai M., Cho K., Hieda J., Todaka Y., Miyazaki T. Mechanical properties of a medical β-type titanium alloy with specific microstructural evolution through high-pressure torsion, Materials Science & Engineering C Materials for Biological Applications 2013; 33(5): 2499.
6. Dorri S., et al. Oxidation kinetics of overstoichiometric $TiB_2$ thin films grown by DC magnetron sputtering. Corrosion Science 2022; 206: 110493.
7. Munro R. G. Material properties of titanium diboride. Journal of Research of the National institute of standards and Technology 2000; 105(5): 709.
8. Xinghong Z., et al. Self-propagating high temperature combustion synthesis of TiB/Ti composites. Materials Science and Engineering: 2003; 348(1–2): 41–46.
9. Lv X., et al. Review on the development of titanium diboride ceramics. Recent Progress in Materials 2024; 6(2): 1–48.
10. Yu B. V. Carbothermic synthesis of titanium diboride: upgrade. Journal of Siberian Federal University. Chemistry 2018; 11(2): 156–166.
11. Krishnarao R. V., and Subrahmanyam J. Studies on the formation of $TiB_2$ through carbothermal

reduction of $TiO_2$ and $B_2O_3$. Materials Science and Engineering: 2003; A 362(1–2): 145–151.

12. Weimer A. W., ed. Carbide, nitride and boride materials synthesis and processing. Springer Science & Business Media, 2012.
13. Hwang Y. and Jong K. L. Preparation of $TiB_2$ powders by mechanical alloying. Materials Letters 2002; 54(1): 1–7.
14. Ge C. L., and Ye R. C. Research on self-propagating eutectic boriding. Journal of materials processing technology 2002; 124(1–2): 14–18.
15. Li X., et al. Low-temperature synthesis of high-purity $TiB_2$ via carbothermal reduction of metatitanic acid and $H_3BO_3$. Ceramics International 2023; 49(24): 40140–40148.
16. Niinomi M., Nakai M., Yonezawa S., Song X., Wang L. Effect of TiB2 or y2o3 additions on mechanical biofunctionality of Ti-29Nb-13Ta-4.6Zr for biomedical applications. Ceramic Transactions. 2011; 228: 75–81. 10.1002/9781118144565.ch8.
17. Zhang L.C., Klemm D., Eckert J., Hao Y.L., Sercombe T.B. Manufacture by selective laser melting and mechanical behavior of a biomedical Ti–24Nb–4Zr–8Sn alloy, Scripta Materialia 2011; 65(1) 21–24.
18. Kafkas F. and Thomas E. Metallurgical and mechanical properties of Ti–24Nb–4Zr–8Sn alloy fabricated by metal injection molding. Journal of Alloys and Compounds 2014; 617: 359–366.
19. Hao Y. L., et al. Super-elastic titanium alloy with unstable plastic deformation. Applied physics letters 2005; 87(9). [20Arisoy, Yiğit M., and Tuğrul Özel. Machine learning based predictive modeling of machining induced microhardness and grain size in Ti–6Al–4V alloy. Materials and Manufacturing Processes 2015; 30(4): 425–433.
20. Gupta B. R. Friction and wear mechanism of polymers, their composites and nanocomposites. Tribology of polymers, polymer composites, and polymer nanocomposites. Elsevier, 2023; 51–117.
21. Mahdi O. S. Preparation and characterization of hydroxyapatite from bovine teeth. Advanced in Natural and Applied Sciences 2017; 11: 623–630.
22. Praveenkumar K., and Kabadi V. R. Realistic Approach to Pin –on- Disc Wear Testing Measurement. International Journal of Advanced Production and Industrial Engineering, 2017; 610: 47–53.
23. Ulusoy U. A review of particle shape effects on material properties for various engineering applications: from macro to nanoscale. Minerals 2023; 13(1): 91.
24. Selvakumar M., et al. Mechanical properties of Titanium–Titanium boride composites through nanoindentation and ultrasonic techniques—an evaluation perspective. Powder Metallurgy and Metal Ceramics 2015; 53557–565.
25. Prakash K., Soorya, et al. Mechanical, corrosion and wear characteristics of powder metallurgy processed Ti-6Al-4V/B4C metal matrix composites. Ain Shams Engineering Journal 2018; 9(4): 1489–1496.
26. Sozhamannan G. G., Mohamed Yusuf G. M., Aravind, Kumaresan G., Velmurugan K., and Venkatachalapathy V. S. K. Effect of applied load on the wear performance of 6061 Al/nano Ticp/Gr hybrid composites. Materials Today: Proceedings 2018; 5(2): 6489–6496.
27. Arul S. Effect of nickel reinforcement on microhardness and wear resistance of aluminum alloy Al7075. Materials Today: Proceedings, 2020; 24: 1042–1051.
28. Hayat, Muhammad D., et al. Titanium metal matrix composites: An overview. Composites Part A: Applied Science and Manufacturing 2019; 121: 418–438.